Electronic Structure of Highly Ruffled Low-Spin Iron(III) Porphyrinates with Electron Withdrawing Heptafluoropropyl Groups at the mesa Positions

ARTICLE *in* INORGANIC CHEMISTRY · OCTOBER 2010

Impact Factor: 4.76 · DOI: 10.1021/ic101184y · Source: PubMed

Article

Electronic Structure of Six-Coordinate Iron(III) Monoazaporphyrins

Kenichiro Nakamura, Akira Ikezaki, Yoshiki Ohgo, Takahisa Ikeue, Saburo Neya, and Mikio Nakamura

Inorg. Chem., **2008**, 47 (22), 10299-10307 • Publication Date (Web): 18 October 2008

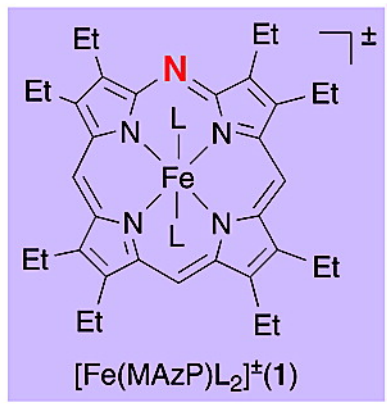

[Fe(MAzP)L$_2$]$^{\pm}$(**1**)

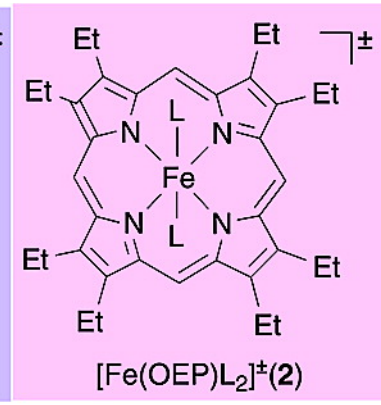

[Fe(OEP)L$_2$]$^{\pm}$(**2**)

	L=^{t}BuNC	L=3,5-Cl$_2$Py
1	S=1/2, $(d_{xy})^2(d_{xz}, d_{yz})^3$	S=3/2 $\rightleftharpoons$ S=1/2
2	S=1/2, $(d_{xz}, d_{yz})^4(d_{xy})^1$	S=5/2, 3/2

More About This Article

Additional resources and features associated with this article are available within the HTML version:

- Supporting Information
- Access to high resolution figures
- Links to articles and content related to this article
- Copyright permission to reproduce figures and/or text from this article

View the Full Text HTML

Inorg. Chem. **2008**, *47*, 10299−10307

Electronic Structure of Six-Coordinate Iron(III) Monoazaporphyrins

Kenichiro Nakamura,[†] Akira Ikezaki,[†] Yoshiki Ohgo,[†,‡] Takahisa Ikeue,[§] Saburo Neya,[||] and Mikio Nakamura*[,†,‡,⊥]

Department of Chemistry, School of Medicine, Toho University, Ota-ku, Tokyo 143-8540, Japan, Research Center of Materials with Integrated Properties, Toho University, Funabashi, 274-8510, Japan, Department of Chemistry, Faculty of Material Science, Shimane University, Department of Physical Chemistry, Graduate School of Pharmaceutical Sciences, Chiba University, Chiba 263-8522, Japan, and Division of Chemistry, Graduate School of Science, Toho University, Funabashi 274-8510, Japan

Received April 16, 2008

The electronic structures of six-coordinate iron(III) octaethylmonoazaporphyrins, $[Fe(MAzP)L_2]^{\pm}$ (**1**), have been examined by means of ^{1}H NMR and EPR spectroscopy to reveal the effect of *meso*-nitrogen in the porphyrin ring. The complexes carrying axial ligands with strong field strengths such as 1-MeIm, DMAP, CN^-, and ^{t}BuNC adopt the low-spin state with the $(d_{xy})^2(d_{xz}, d_{yz})^3$ ground state in a wide temperature range where the ^{1}H NMR and EPR spectra are taken. In contrast, the complexes with much weaker axial ligands, such as 4-CNPy and 3,5-Cl_2Py, exhibit the spin transition from the mainly $S = 3/2$ at 298 K to the $S = 1/2$ with the $(d_{xy})^2(d_{xz}, d_{yz})^3$ ground state at 4 K. Only the THF complex has maintained the $S = 3/2$ throughout the temperature range examined. Thus, the electronic structures of **1** resemble those of the corresponding iron(III) octaethylporphyrins, $[Fe(OEP)L_2]^{\pm}$ (**2**). A couple of differences have been observed, however, in the electronic structures of **1** and **2**. One of the differences is the electronic ground state in low-spin bis(^{t}BuNC) complexes. While $[Fe(OEP)(^tBuNC)_2]^+$ adopts the $(d_{xz}, d_{yz})^4(d_{xy})^1$ ground state, like most of the bis(^{t}BuNC) complexes reported previously, $[Fe(MAzP)(^tBuNC)_2]^+$ has shown the $(d_{xy})^2(d_{xz}, d_{yz})^3$ ground state. Another difference is the spin state of the bis(3,5-Cl_2Py) complexes. While $[Fe(OEP)(3,5\text{-}Cl_2Py)_2]^+$ has maintained the mixed $S = 3/2$ and 5/2 spin state from 298 to 4 K, $[Fe(MAzP)(3,5\text{-}Cl_2Py)_2]^+$ has shown the spin transition mentioned above. These differences have been ascribed to the narrower N4 cavity and the presence of lower-lying π^* orbital in MAzP as compared with OEP.

Introduction

The spin state and electron configuration of ferric porphyrin complexes are controlled by various factors including the nature and number of axial ligands, electronic effects of peripheral substituents, deformation and core modification of the porphyrin ring, etc.[1−5] By manipulating these factors, we are now able to obtain various iron(III) porphyrins with unusual electronic structures.[6] For example, we have recently reported that low-spin bis(^{t}BuNC) complex of diazaporphyrin, $[Fe(DAzP)(^tBuNC)_2]ClO_4$, adopts the $(d_{xy})^2(d_{xz}, d_{yz})^3$ ground state.[2,5,7,8] This is quite unusual because all the

* To whom correspondence should be addressed. E-Mail: mnakamu@med.toho-u.ac.jp.
† Department of Chemistry, School of Medicine, Toho University.
‡ Research Center of Materials with Integrated Properties, Toho University.
§ Department of Chemistry, Faculty of Material Science, Shimane University.
|| Department of Physical Chemistry, Graduate School of Pharmaceutical Sciences, Chiba University.
⊥ Division of Chemistry, Graduate School of Science, Toho University.

(1) Scheidt, W. R. In *The Porphyrin Handbook*; Kadish, K. M., Smith, K. M., Guilard, R., Eds.;Academic Press: San Diego, CA, 2000; Vol. *3*, Chapter 16, pp. 49−112.
(2) Walker, F. A. In *The Porphyrin Handbook*; Kadish, K. M., Smith, K. M., Guilard, R., Eds.; Academic Press, San Diego, CA, 2000; Vol. *5*, Chapter 36, pp 81−183.
(3) Walker, F. A. *Inorg. Chem.* **2003**, *42*, 4526–4544.
(4) Walker, F. A. *Chem. Rev.* **2004**, *104*, 589–615.
(5) Nakamura, M. *Coord. Chem. Rev.* **2006**, *250*, 2271–2294.
(6) Nakamura, M.; Ohgo, Y.; Ikezaki, A. *J. Inorg. Biochem.* **2008**, *102*, 433–445.
(7) OEP, dianion of 2,3,7,8,12,13,17,18-octaethylporphyrin; MAzP, dianion of 2,3,7,8,12,13,17,18-octaethyl-5-azaporphyrin; DAzP, dianion of 2,7,12,18-tetrabutyl-3,7,13,17-tetramethyl-5,15-diazaporphyrine; OMTPP, dianion of 2,3,7,8,12,13,17,18-octamethyl-5,10,15,20-tetraphenylporphyrin; OETPP, dianion of 2,3,7,8,12,13,17,18-octaethyl-5,10,15,20-tetraphenylporphyrin; DMAP, 4-(N,N-dimethylamino)-pyridine; 1-MeIm, 1- methylimidazole; 4-CNPy, 4-cyanopyridine; 3,5-Cl_2Py, 3,5-dichloropyridine; ^{t}BuNC, *tert*-butylisocyanide.

10.1021/ic800674d CCC: $40.75
Published on Web 10/18/2008

Scheme 1. Six-Coordinate $[Fe(DAzP)L_2]^{\pm}$, $[Fe(MAzP)L_2]^{\pm}$(**1**), and $[Fe(OEP)L_2]^{\pm}$(**2**)

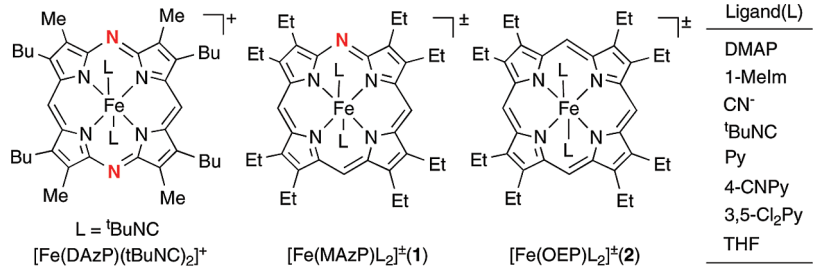

bis(^{t}BuNC) complexes of porphyrins, $[Fe(Por)(^tBuNC)_2]^+$, exhibit the $(d_{xz}, d_{yz})^4(d_{xy})^1$ ground state.[9,10] The unexpected electronic ground state of $[Fe(DAzP)(^tBuNC)_2]ClO_4$ suggests that the substitution of two *meso*-carbon atoms by nitrogen atoms should greatly affect the electronic structure of iron(III) porphyrins. As an extension of our continuous project to elucidate the factors that affect the electronic structure of metal porphyrins,[5,6,11−13] we have considered it quite important to reveal how the nitrogen atom at the meso position perturbs the electronic structure of iron(III) porphyrins.[14,15] As for the electronic structure of iron(III) monoazaporphyrin, Balch and co-workers reported that both five-coordinate Fe(MAzP)Cl and six-coordinate $[Fe(MAzP)(DMSO)_2]^+$ and $[Fe(MAzP)Cl_2]^-$ adopt the high-spin state.[16] In the present study, we have prepared a series of six-coordinate iron(III) monoazaporphyrins, $[Fe(MAzP)L_2]^{\pm}$ (**1**), and have examined the electronic structure by means of ^{1}H NMR and EPR spectroscopy. The purpose of this study is to compare the electronic structures of **1** with those of the corresponding $[Fe(OEP)L_2]^+$(**2**) to reveal the effect of the *meso*-nitrogen atom. The axial ligands (L) examined are DMAP, 1-MeIm, CN^-, ^{t}BuNC, Py, 4-CNPy, 3,5-Cl_2Py, and THF. In this paper, each complex is signified as **1**(DMAP), **1**(3,5-Cl_2Py), and **2**(^{t}BuNC), etc.

Experimental Section

Synthesis. Fe(MAzP)Cl was prepared according to the literature methods.[16−18] UV−vis and ^{1}H NMR spectra were essentially the same as those reported by Balch and co-workers.[16] ^{1}H NMR (CD_2Cl_2, 298 K): The CH_2 protons showed eight signals, each corresponding to 2H, at 48.4, 47.7, 46.0, 45.2, 44.8, 44.1, 40.0 and 39.0 ppm. The CH_3 protons showed three signals at 7.5(6H), 7.3(6H), and 6.9(12H) ppm. The *meso*-H signals appeared at −18.2(1H) and −26.4(2H) ppm.

$[Fe(MAzP)(THF)_2]ClO_4$. A mixture of Fe(MAzP)Cl(17.7 mg, 2.83×10^{-5} mol) and $AgClO_4$ (5.87 mg, 2.83×10^{-5} mol) was placed in a vial under argon atmosphere, to which 10 mL of THF was added. The THF solution was stirred for 15 min and was then filtered to remove the solid produced during the reaction.[19] **Caution!** *Perchlorate salts are potentially explosive when heated or shocked. Handle them in milligram quantities with care.* After the evaporation of THF, dichloromethane was added to the solid, and the solution was filtered again. The filtrate was evaporated, and the brown solid thus obtained was dried in vacuo for 3 h at 25 °C. The CD_2Cl_2 solution of the solid was placed in an NMR sample tube, to which was added 6 equiv of THF to form $[Fe(MAzP)(THF)_2]ClO_4$. ^{1}H NMR(CD_2Cl_2, 298 K, δ): 32.1(4H, 2 × CH_2), 30.5(4H, 2 × CH_2), 29.7(4H, 2 × CH_2), 27.7(4H, 2 × CH_2), 4.7(24H, 8 × CH_3), 24.3(2H, 2 × *meso*-H), 27.6(1H, *meso*-H) ppm.

$[Fe(MAzP)L_2]X$ (1). L = DMAP, 1-MeIm, CN^-, Py, 4-CNPy, 3,5-Cl_2Py, ^{t}BuNC. X = ClO_4^-, Bu_4N^+. NMR samples for a series of six-coordinated $[Fe(MAzP)L_2]^{\pm}$ (**1**) were prepared by the addition of 4−6 equiv of the ligands (L) to the CD_2Cl_2 solution of $Fe(MAzP)ClO_4$ or Fe(MAzP)Cl. Formation of **1** was confirmed in each experiment by the titration of the ligand solution; ligand solution was added until no appreciable change in chemical shifts was observed.

Spectral Measurement. UV−vis spectra were recorded on a Shimadzu MultiSpec-1500 spectrophotometer. ^{1}H NMR spectra were recorded on a JEOL LA300 spectrometer operating at 300.4 MHz for ^{1}H. Chemical shifts were referenced to the residual peaks of CD_2Cl_2 (δ 5.32 ppm). EPR spectra were recorded on a Bruker EMX Plus or E500 spectrometer operating at X band and equipped with an Oxford helium cryostat.

Magnetic Moments. Solution magnetic moments were measured by the Evans method in CD_2Cl_2 solution using CH_2Cl_2 as the chemical shift reference.[20] The magnetic moments(μ_{eff}^1) of **1** (3,5-Cl_2Py) were determined at various temperatures relative to that of high-spin Fe(OEP)Cl ($\mu_{eff}^2 = 5.92\ \mu_B$) according to $\mu_{eff}^1 = (\Delta\nu^1/\Delta\nu^2)^{1/2}\mu_{eff}^2$.[21]

Molecular Orbital Calculations. To reveal how the molecular orbitals of monoazaporphyrin are different from those of porphyrin, the molecular orbital calculation of unsubstituted zinc(monoazaporphin) and zinc(porphin) complexes was carried out. Molecular structures of these complexes were first determined by the semiem-

(8) Ohgo, Y.; Neya, S.; Uekusa, H.; Nakamura, M. *Chem. Commun.* **2006**, 4590–4592.
(9) More recently, we have reported that highly saddled complex with electron withdrawing aryl groups at the meso positions, $[Fe(OETArP)(^tBuNC)_2]^+$, adopts the $(d_{xy})^2(d_{xz}, d_{yz})^3$ ground state despite the coordination of ^{t}BuNC ligand.[10]
(10) Ohgo, Y.; Hoshino, A.; Okamura, T.; Uekusa, H.; Hashizume, D.; Ikezaki, A.; Nakamura, M. *Inorg. Chem.* **2007**, *46*, 8193–8207.
(11) Ikezaki, A.; Nakamura, M. *Inorg. Chem.* **2003**, *42*, 2301–2310.
(12) Ikezaki, A.; Nakamura, M. *Chem. Lett.* **2005**, *34*, 1046–1047.
(13) Ikezaki, A.; Nakamura, M.; Cheng, R.-J. *Chem. Lett.* **2006**, *35*, 156–157.
(14) For the review on *meso*-azaporphyrins, see ref 15.
(15) Kobayashi, N. In *The Porphyrin Handbook*; Kadish, K. M., Smith, K. M., Guilard, R., Eds.; Academic Press: San Diego, CA, 2000; Vol. *2*, Chapter 13, pp 301−360.
(16) Balch, A. L.; Olmstead, M. M.; Safari, N. *Inorg. Chem.* **1993**, *32*, 291–296.
(17) Saito, S.; Tamura, N. *Bull. Chem. Soc. Jpn.* **1987**, *60*, 4037–4049.
(18) Saito, S.; Sumita, S.; Iwai, K.; Sano, H. *Bull. Chem. Soc. Jpn.* **1988**, *61*, 3539–3547.
(19) Ikeue, T.; Ohgo, Y.; Saitoh, T.; Yamaguchi, T.; Nakamura, M. *Inorg. Chem.* **2001**, *40*, 3423–3434.
(20) Evans, D. F.; James, T. A. *J. Chem. Soc., Dalton Trans.* **1979**, 723–726.
(21) Groves, J. T.; Quinn, R.; McMurry, T. J.; Nakamura, M.; Lang, G.; Boso, B. *J. Am. Chem. Soc.* **1985**, *107*, 354–360.

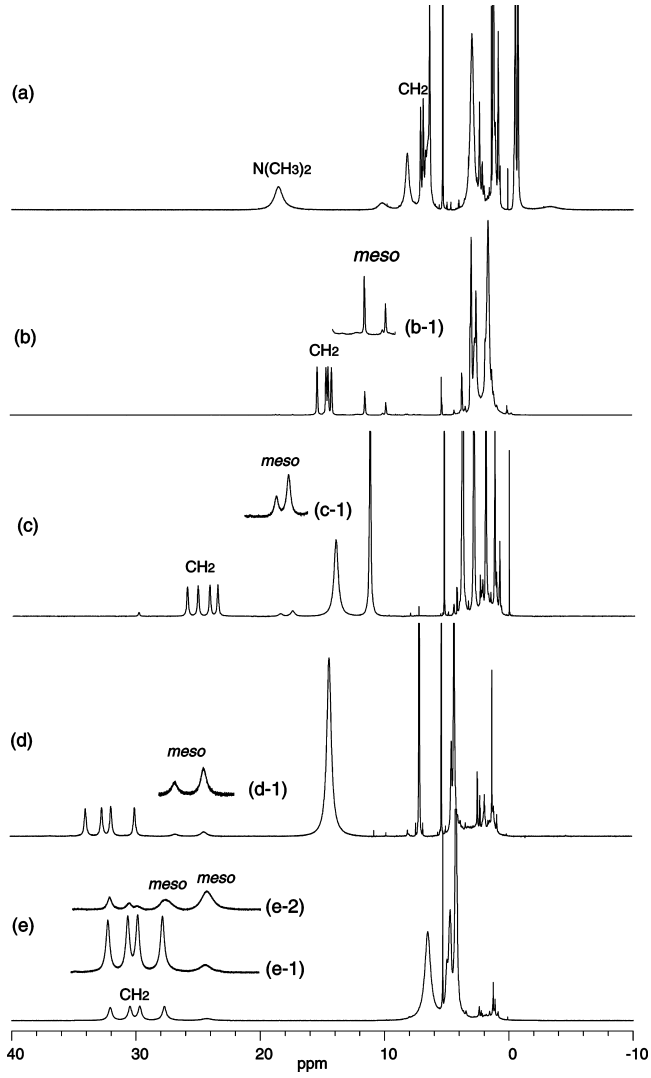

Figure 1. ^{1}H NMR spectra of $[Fe(MAzP)L_2]^+$(**1**) taken in CD_2Cl_2 solution at 298 K, where L is (a) DMAP, (b) ^{t}BuNC, (c) 4-CNPy, (d) 3,5-Cl_2Py, and (e) THF. Insets b-1, c-1, d-1, and e-1 are expansion of the *meso*-H reagion. Inset e-2: Inversion recoverly measurement with $\tau = 2.65$ ms.

pirical PM3, which was then optimized by the density function theory (DFT) calculation at the B3LYP level with 6−31G* basis set.[22,23]

Results

^{1}H NMR Spectra of a Series of $[Fe(MAzP)L_2]^{\pm}$ (1). Figure 1a−e shows the ^{1}H NMR spectra of the six-coordinate complexes such as (a) **1**(DMAP), (b)**1**(^{t}BuNC), (c) **1**(4-CNPy), (d) **1**(3,5-Cl_2Py), and (e) **1**(THF); the ^{1}H NMR spectra of the other complexes are shown in the Supporting Information. In each spectrum, the CH_2 and *meso*-H signals are labeled. In the case of **1**(THF) shown in Figure 1e, only one of the *meso*-H signal corresponding to 2H was observed at 24.3 ppm; the other *meso*-H(1H) signal was hidden behind the CH_2 signals. We were able to observe this signal at 27.6 ppm by applying the inversion−recovery method with pulse interval 2.65 ms as shown in inset (e-2). Table 1 lists the chemical shifts of a series of **1** and **2** determined at 298 (upper) and 223 K(lower). Figure 2a) shows the Curie plots of the pyrrole−CH_2 signals of some selected complexes of **1**. While **1**(DMAP), **1**(^{t}BuNC), and **1**(THF) exhibited good linearity, other complexes such as **1**(1-MeIm) and **1**(CN^-) showed a slight curvature; Curie plots of **1**(1-MeIm), **1**(^{t}BuNC), and **1**(CN^-) are given in the Supporting Information. A considerable curvature was observed in the case of **1**(4-CNPy) and**1**(3,5-Cl_2Py). Similar temperature dependence was observed in the ^{1}H NMR signals of $[Fe(OEP)L_2]^{\pm}$ (**2**) as shown in Figure 2b. Figure 3a shows the Curie plots of the *meso*-H signals of some selected complexes of **1**. As in the case of the CH_2 signals, **1**(DMAP) and **1**(THF) showed good linearity though the chemical shifts of one of the *meso*-H signals of **1**(THF) were unable to determine below 273 K because of the broadening. The other complexes such as **1**(4-CNPy) and**1**(3,5-Cl_2Py) exhibited a considerable curvature. Similar temperature dependence was observed in the Curie plots of the *meso*-H signals of **2** as shown in Figure 3b. Figure 4a and b show the Curie plots of the CH_3 signals in **1** and **2**, respectively. In both systems, bis(DMAP) and bis(THF) showed linear lines with negative and positive slopes, respectively. Another characteristic feature is that the CH_3 signals in **1**(3,5-Cl_2Py) and **1**(4-CNPy) appeared more upfield than those of **2**(3,5-Cl_2Py) and **2**(4-CNPy). Figure 5a shows the comparison of the Curie plots of some signals in **1**(^{t}BuNC) and **2**(^{t}BuNC). Although the ^{1}H NMR chemical shifts and the temperature dependence of the signals in **1** and **2** carrying the same axial ligands were in most cases quite similar, as shown in Figures 2−4, those of **1**(^{t}BuNC) and **2**(^{t}BuNC) were completely different. The largest difference was observed in the *meso*-H signals as shown in Figure 5b. The difference in chemical shifts reached as much as 70 ppm at 223 K.

EPR Spectra of a Series of $[Fe(MAzP)L_2]^{\pm}$ (1). Figure 6 shows the EPR spectra of (a) **1**(DMAP), (b) **1**(1-MeIm), (c) **1**(^{t}BuNC), (d)**1**(4-CNPy), and (e) **1**(THF). These spectra were taken in frozen CH_2Cl_2 solution at 4−20 K. As shown in Figure 6, the EPR spectrum of each complex contains some weak signals at 4.3−4.5 ascribed to the non-heme iron(III) ions. A sharp signal at $g = 5.9$ in Figure 6a and e is ascribed to high-spin Fe(MAzP)Cl contaminated in the sample. Table 2 lists the EPR g values of the major components of **1** and **2**.

Molecular Orbital Calculation. The frontier molecular orbitals of zinc(II) monoazaporphin complex with C_{2v} symmetry are shown in Figure 7. The results are consistent with the previous work done by Kobayashi and co-workers.[24,25] The HOMO and HOMO−1 are similar to the a_{1u} and a_{2u} orbitals of the D_{4h} porphin, respectively. As in the case of porphin, monoazaporphin has two orbitals near the HOMO that can interact with the iron d_π orbitals. They are HOMO−3 and HOMO−4 with nearly the same energy

(22) *Spartan* '04 Software; Wavefunction, Inc: Irvine, CA, 2004.
(23) Ghosh, A. In *The Porphyrin Handbook*; Kadish, K. M.; Smith, K. M.; Guilard, R., Eds.; Academic Press: San Diego, CA, 2000; Vol. 7, Chapter 47, pp 1−28.
(24) Kobayashi, N.; Nakajima, S.; Ogata, H.; Fukuda, T. *Chem.−Eur. J.* **2004**, *10*, 6294–6312.
(25) Ogata, H.; Fukuda, T.; Nakai, K.; Fujimura, Y.; Neya, S.; Stuzhin, P. A.; Kobayashi, N. *Eur. J. Inorg. Chem.* **2004**, 1621–1629.

Table 1. ^{1}H NMR Chemical Shifts of **1** and **2** Taken in CD_2Cl_2 Solution at 298 (Upper) and 223 K(Lower)

$[Fe(MAzP)L_2]^{\pm}$ (**1**)

ligands	CH_2				(ave)	CH_3(ave)	m(1H)[a]	m(2H)[a]	(ave)
DMAP	6.38	6.38	6.89	7.10	(6.69)	(−0.63)	1.50[b]	2.41[b]	(2.11)
	4.86	5.03	6.21	6.45	(5.64)	(−2.59)	−5.43	−3.18	(−3.93)
1-Melm	6.57	6.68	7.38	7.70	(7.08)	(−0.42)			
	5.53	5.53	7.99	8.35	(6.85)	(−1.65)			
CN^-	5.78	6.03	6.47	6.73	(6.25)	(−1.59)	−0.20	1.90	(1.20)
	4.64	5.36	5.36	6.27	(5.41)	(−2.81)	−7.72	−3.78	(−5.09)
^{t}BuNC	14.17	14.44	14.61	15.32	(14.64)	(2.73)	9.79	11.47	(10.91)
	16.48	16.75	16.80	18.14	(17.04)	(4.28)	10.74	13.68	(12.70)
Py	10.27	10.60	10.93	11.26	(10.77)	(0.01)	2.82	4.17	(3.72)
	8.11	8.78	9.62	9.67	(9.05)	(−2.15)	−5.73	−3.05	(−3.94)
4-CNPy	23.52	24.15	25.10	25.96	(24.68)	(3.83)	18.48	17.50	(17.83)
	15.16	13.54	14.84	15.46	(14.72)	(−0.71)	−0.32	2.04	(1.25)
3,5-Cl_2Py	30.01	31.89	32.64	33.95	(32.12)	(4.27)	26.75	24.45	(25.22)
	33.54	34.96	36.70	37.74	(35.74)	(4.17)	30.05	28.36	(28.94)
THF	27.75	29.74	30.50	32.10	(30.02)	(4.73)	27.6	24.3	(26.54)
	33.30	34.91	36.77	38.14	(35.78)	(5.65)			

$[Fe(OEP)L_2]^{\pm}$ (**2**)

ligands	CH_2	CH_3	*meso*[a]
DMAP	6.73	−0.41	1.82
	4.64	−1.49	−4.60
1-Melm	7.06	−0.24	2.90
	5.82	−1.56	−0.82
CN^-	5.63	−0.66	0.72
	4.58	−2.59	−5.04
^{t}BuNC	7.61	3.19	−37.71
	7.40	3.18	−58.17
Py	14.71	1.26	7.00
	8.50	−0.25	−3.83
4-CNPy	28.06	4.11	20.45
	15.10	0.62	0.84
3,5-Cl_2Py	38.8	6.27	32.0
	46.3	7.7	46.3
THF	38.13	6.20	39.50
	50.51	8.13	60.04

[a] m(1H), m(2H): *meso*-H signals corresponding to 1H and 2H, respectively. [b] Extrapolated values from low tempearutre.

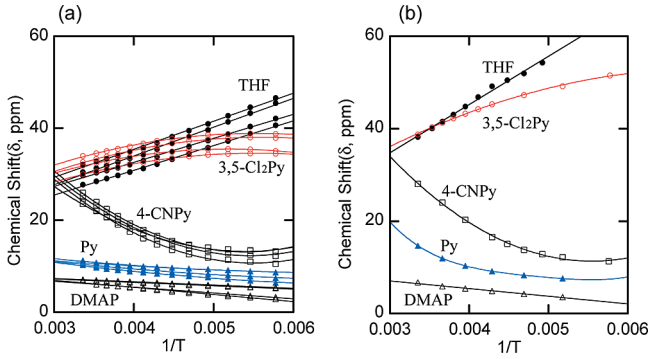

Figure 2. Curie plots of the CH_2 signals of (a) **1** and (b) **2**.

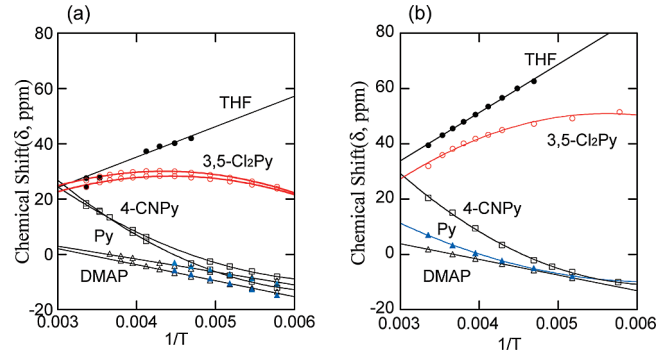

Figure 3. Curie plots of the meso-H signals in (a) **1** and (b) **2**.

levels. Both orbitals have major electron densities on the pyrrole nitrogen and β carbon atoms. The LUMO and LUMO+1 can also interact with the iron d_π orbitals, which as in the case of porphin have relatively large coefficients on the *meso*-carbon atoms. The molecular orbitals of monoazaporphin having a large coefficient at the *meso*-nitrogen atom, such as HOMO−1, LUMO, and LUMO+1, are much more stable than the corresponding orbitals in porphin. In contrast, the molecular orbitals with only a small coefficient at the *meso*-nitrogen, such as HOMO, HOMO−3, and HOMO−4, are not much stabilized as compared with the corresponding orbitals in porphin.

Discussion

Determination of the Electronic Structure of $[Fe(MAzP)L_2]^{\pm}$ (1). ^{1}H NMR Spectroscopy. Iron(III) porphyrins usually adopt either a high-spin ($S = 5/2$) or low-spin ($S = 1/2$) state.[1,26] Recent studies have revealed, however, that some complexes adopt an essentially pure intermediate-spin ($S = 3/2$) state, if the complexes have extremely weak axial ligands or a highly deformed porphyrin core.[5,27−34] Generally speaking, iron(III) porphyrins can not

(26) Scheidt, W. R.; Reed, C. A. *Chem. Rev.* **1981**, *81*, 543–555.
(27) Reed, C. A.; Guiset, F. *J. Am. Chem. Soc.* **1996**, *118*, 3281–3282.

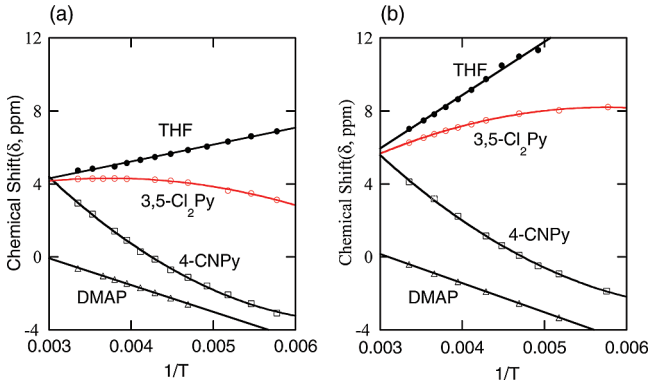

Figure 4. Curie plots of the CH_3 signals in (a) **1** and (b) **2**.

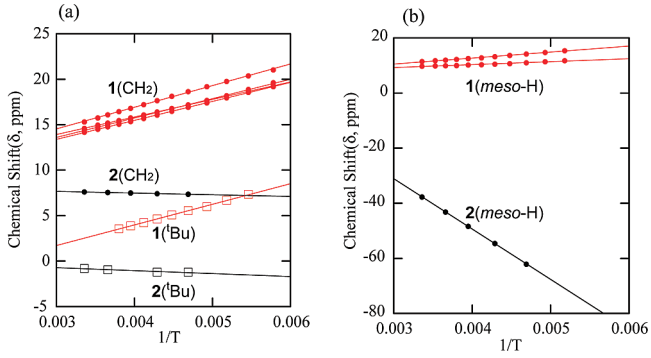

Figure 5. Compariosn of the Curie plots of some signals in bis(tBuNC) complexes of **1** and **2**. Red and black simbols signify **1** and **2**, respectively: (a) CH_2 (filled circle) and *t*-butyl(open square) signals and (b) *meso*-H signals.

always exist as a pure single spin state. In some cases, they exist as an equilibrium mixture between $S = 1/2$ and 5/2,[35−38] $S = 1/2$ and 3/2,[5,39−41] and $S = 3/2$ and 5/2.[42−44] Furthermore, some of the low-spin complexes switch their electron configuration between $(d_{xy})^2(d_{xz}, d_{yz})^3$ and $(d_{xz},d_{yz})^4(d_{xy})^1$.[5,45−47] ^{1}H NMR spectroscopy is a powerful method to determine the spin state at 173−373 K because the chemical shifts of the peripheral and axial ligand signals reflect the spin states of the iron(III) ions.[2−5]

As listed in Table 1, the complexes carrying axial ligands with strong field strength such as **1**(DMAP), **1**(1-MeIm), and **1**(CN^-) exhibited the CH_2 signals at the downfield positions, 6−8 ppm, and the *meso*-H signals at the upfield positions, 1−3 ppm. In addition, the CH_2 and *meso*-H signals of these complexes showed fairy good linearity in the Curie plots. The ^{1}H NMR characteristics mentioned above suggest that these complexes adopt the low-spin state with the $(d_{xy})^2(d_{xz}, d_{yz})^3$ ground state. Namely, the small downfield shifts

(28) Evans, D. R.; Reed, C. A. *J. Am. Chem. Soc.* **2000**, *122*, 4660–4667.
(29) Simonato, J.-P.; Pécaut, J.; Le Pape, L.; Oddou, J.-L.; Jeandey, C.; Shang, M.; Scheidt, W. R.; Wojaczyński, J.; Wołowiec, S.; Latos-Grażyński, L.; Marchon, J.-C. *Inorg. Chem.* **2000**, *39*, 3978–3987.
(30) Ikeue, T.; Saitoh, T.; Yamaguchi, T.; Ohgo, Y.; Nakamura, M.; Takahashi, M.; Takeda, M. *Chem. Commun* **2000**, 1989–1990.
(31) Ohgo, Y.; Saitoh, T.; Nakamura, M. *Acta Crystallogr.* **2001**, *C57*, 233–234.
(32) Nakamura, M.; Ikeue, T.; Ohgo, Y.; Takahashi, M.; Takeda, M. *Chem. Commun* **2002**, 1198–1199.
(33) Sakai, T.; Ohgo, Y.; Hoshino, A.; Ikeue, T.; Saitoh, T.; Takahashi, M.; Nakamura, M. *Inorg. Chem.* **2004**, *43*, 5034–5043.
(34) Hoshino, A.; Ohgo, Y.; Nakamura, M. *Inorg. Chem.* **2005**, *44*, 7333–7344.

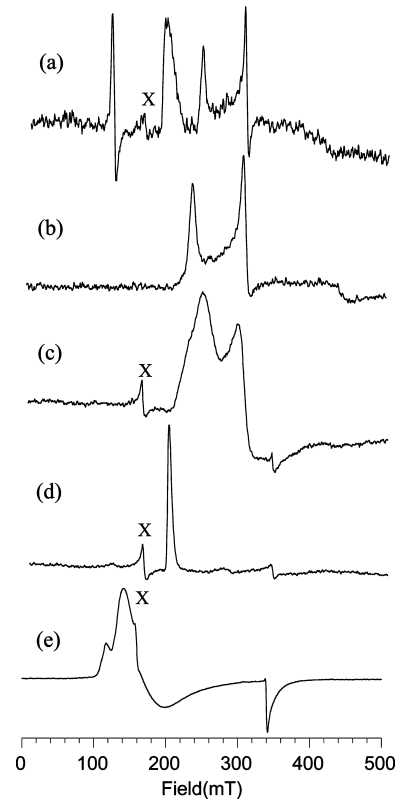

Figure 6. EPR spectra of **1** where L is (a) DMAP, (b) 1-MeIm, (c)^{t}BuNC, (d) 4-CNPy, and (e) THF. Signals signified by X are ascribed to the nonheme iron.

Table 2. EPR *g* Values of **1** and **2** Taken in Frozen CH_2Cl_2 Solutions at 4−20 K

complexes	*g* values			ref
[Fe(MAzP)L$_2$]*(**1**)				
DMAP[a]	3.62			tw
	2.83	2.24	1.61	
1-MeIm[b]	2.94	2.24	1.53	tw
CN^-	3.41			tw
^{t}BuNC	2.84	2.26	1.58	tw
Py	3.45			
	2.4	2.1		tw
4-CNPy[c]	3.48			tw
3,5-Cl$_2$Py[d]	3.46			tw
THF	4.26		1.99	tw
[Fe(OEP)L$_2$]*(**2**)				
DMAP	2.81	2.28	1.64	48, 61
1-MeIm	2.99	2.27	1.51	2
CN^-	3.73			2
^{t}BuNC	2.25		1.83	49
Py	3.46			tw
4-CNPy	3.29			tw
3,5-Cl$_2$Py	4.23		2.00	58
THF	4.39		1.99	tw[e]

[a−d] *g* values of minor components. [a] 5.88, 4.25. [b] 6.12, 5.55, 4.25, 2.0. [c] 4.25. [d] 6.12, 5.65, 4.25, 1.8. [e] Originally reported by Masuda et al.[62]

of the CH_2 signals can be explained in terms of the interaction between the half-filled iron d_π and the filled $3e_g$-like orbitals of MAzP; the $3e_g$-like orbitals correspond to the HOMO−3 and HOMO−4 in Figure 7 in the case of **1**. The upfield shift of the *meso*-H signals should mainly be caused by the dipolar contribution in the $(d_{xy})^2(d_{xz}, d_{yz})^3$ type complexes.[2−5] The similarity of the CH_2 and *meso*-H chemical shifts of **1**(DMAP), **1**(1-MeIm), and **1**(CN^-) to those of **2**(DMAP)

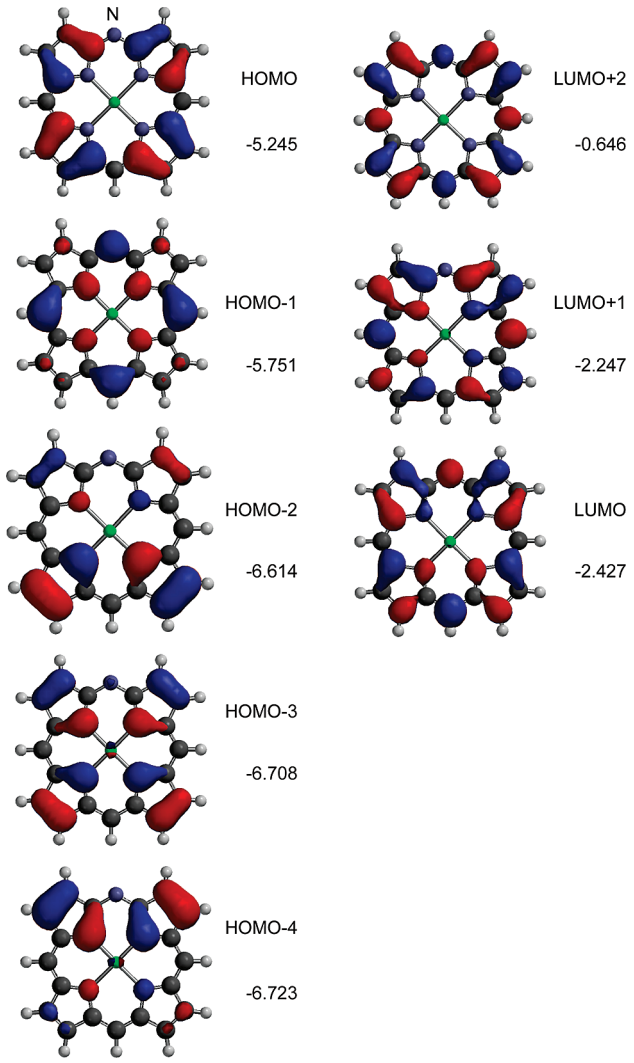

Figure 7. Frontier orbitals and orbital energies (eV) in Zn(monoazaporphyrin) with C_{2v} symmetery.

further supports the $(d_{xy})^2(d_{xz},d_{yz})^3$ ground state; **2**(DMAP) is known to adopt the $(d_{xy})^2(d_{xz}, d_{yz})^3$ ground state.[48]

The bis(ᵗBuNC) complex, **1**(ᵗBuNC), is quite unique because both the α-CH_2 and *meso*-H signals shifted more downfield than those of other low-spin complexes with the $(d_{xy})^2(d_{xz}, d_{yz})^3$ ground state, such as **1**(DMAP), **1**(1-MeIm), and **1**(CN^-). The average chemical shifts for the α-CH_2 and *meso*-H signals of **1**(ᵗBuNC) are 14.6 and 10.9 ppm, respectively, while those of **1**(DMAP) are 6.7 and 2.1 ppm, respectively, as listed in Table 1. The results suggest that the pyrrole β and *meso*-carbon atoms in **1**(ᵗBuNC) have much larger positive and negative spin, respectively, than those in the other low-spin complexes with the $(d_{xy})^2(d_{xz}, d_{yz})^3$ ground state. Furthermore, the ^{1}H NMR chemical shifts in **1**(ᵗBuNC) are completely different from those of other bis(ᵗBuNC) complexes reported previously. For example, the α-CH_2 and *meso*-H signals of **2**(ᵗBuNC) appeared at 7.6 and −37.7 ppm, respectively.[49] Considering the fact that **2**(ᵗBuNC) is a low-spin complex with the $(d_{xz}, d_{yz})^4(d_{xy})^1$ ground state,[49] it should be reasonable to conclude that **1**(ᵗBuNC) is the low-spin complex with the $(d_{xy})^2(d_{xz}, d_{yz})^3$ ground state in spite of the bis(ᵗBuNC) coordination.[8,10] The low-spin $(d_{xy})^2(d_{xz}, d_{yz})^3$ ground state of **1**(ᵗBuNC) is maintained in the temperature range between 298 and 173 K since the Curie plots of the CH_2 and *meso*-H signals exhibited excellent linearity as shown in Figure 5.

The $CH_2$and *meso*-H signals of **1**(4-CNPy) and **1**(3,5-Cl_2Py) appeared much more downfield than those of the low-spin complexes with the $(d_{xy})^2(d_{xz}, d_{yz})^3$ ground state; the chemical shifts of the CH_2 and *meso*-H signals of **1**(3,5-Cl_2Py) reached as much as 32.1 (av) and 25.2 (av) ppm, respectively, at 298 K. The large downfield shift of the CH_2 signals at 298 K suggests that these complexes are either in the $S = 3/2$ spin state with two unpaired electrons in the d_π orbitals or in the $S = 5/2$ spin state with an unpaired electron in the $d_{x^2-y^2}$ orbital. It is difficult to differentiate the $S = 5/2$ from the $S = 3/2$ spin state on the basis of the CH_2 chemical shifts because they appear fairly downfield both in the $S = 3/2$ and 5/2 complexes.[30] We considered that the chemical shifts of the β-CH_3 signals and their temperature dependence should be a good probe to recognize the spin states because the $S = 5/2$ complexes exhibit the β-CH_3 signals more downfield than the $S = 3/2$ complexes; the unpaired electron can be delocalized to the CH_3 protons through σ-bonds in the $S = 5/2$ complexes. The data in Table 1 indicates that the CH_3 signals of **1**(4-CNPy) and **1**(3,5-Cl_2Py) appear at 3.8 and 4.3 ppm, respectively. Since the CH_3 signals of high-spin Fe(MAzP)Cl appear at 6.9−7.5 ppm, it should be reasonable to conclude that they are mainly in the $S = 3/2$. As shown in Figures 2 and 3, the CH_2 and *meso*-H signals of **1**(4-CNPy) showed large upfield shifts as the temperature was lowered and approached to those of low-spin **1**(DMAP). The result can be explained in terms of the spin transition from the mainly $S = 3/2$ to the mainly $S = 1/2$ state. Similar temperature dependence was observed in **1**(3,5-Cl_2Py), though the degree of the spin transition was much smaller; the CH_2 signals appeared still extremely downfield, 35.7 ppm

(35) Beetlestone, J.; George, P. *Biochemistry* **1964**, *3*, 707–714.
(36) Scheidt, W. R.; Geiger, D. K.; Haller, K. J. *J. Am. Chem. Soc.* **1982**, *104*, 495–499.
(37) Ellison, M. K.; Nasri, H.; Xia, Y.-M.; Marchon, J.-C.; Schulz, C. E.; Debrunner, P. G.; Scheidt, W. R. *Inorg. Chem.* **1997**, *36*, 4804–4811.
(38) Neya, S.; Tsubaki, M.; Hori, H.; Yonetani, T.; Funasaki, N. *Inorg. Chem.* **2001**, *40*, 1220–1225.
(39) Ikeue, T.; Ohgo, Y.; Yamaguchi, T.; Takahashi, M.; Takeda, M.; Nakamura, M. *Angew. Chem., Int. Ed.* **2001**, *40*, 2617–2620.
(40) Ohgo, Y.; Ikeue, T.; Nakamura, M. *Inorg. Chem.* **2002**, *41*, 1698–1700.
(41) Ikeue, T.; Ohgo, Y.; Ongayi, O.; Vicente, M. G. H.; Nakamura, M. *Inorg. Chem.* **2003**, *42*, 5560–5571.
(42) Ohgo, Y.; Chiba, Y.; Hashizume, D.; Uekusa, H.; Ozeki, T.; Nakamura, M. *Chem. Commun.* **2006**, 1935–1937.
(43) Neya, S.; Takahashi, A.; Ode, H.; Hoshino, T.; Hata, M.; Ikezaki, A.; Ohgo, Y.; Takahashi, M.; Hiramatsu, H.; Kitagawa, T.; Furutani, Y.; Kandori, H.; Funasaki, N.; Nakamura, M. *Eur. J. Inorg. Chem.* **2007**, 3188–3194.
(44) Neya, S.; Takahashi, A.; Ode, H.; Hoshino, T.; Ikezaki, A.; Ohgo, Y.; Takahashi, M.; Furutani, Y.; Lórentz-Fonfría, V. A.; Kandori, H.; Hiramatsu, H.; Kitagawa, T.; Teraoka, J.; Funasaki, N.; Nakamura, M. *Bull. Chem. Soc. Jpn.* **2008**, *81*, 136–141.
(45) Ikeue, T.; Ohgo, Y.; Saitoh, T.; Nakamura, M.; Fujii, H.; Yokoyama, M. *J. Am. Chem. Soc.* **2000**, *122*, 4068–4076.
(46) Ikezaki, A.; Nakamura, M. *Inorg. Chem.* **2002**, *41*, 2761–2768.
(47) Ikezaki, A.; Ikeue, T.; Nakamura, M. *Inorg. Chim. Acta* **2002**, *335*, 91–99.
(48) Ikeue, T.; Yamaguchi, T.; Ohgo, Y.; Nakamura, M. *Chem. Lett.* **2000**, 342–343.
(49) Walker, F. A.; Nasri, H.; Turowska-Tyrk, I.; Mohanrao, K.; Watson, C. T.; Shokhirev, N. V.; Debrunner, P. G.; Scheidt, W. R. *J. Am. Chem. Soc.* **1996**, *118*, 12109–12118.

in average, even at 223 K. Change in spin state has also been confirmed by the temperature dependence of the effective magnetic moments. The effective magnetic moment of **1**(3,5-Cl_2Py) was determined by the Evans method to be 4.0 μ_B in CD_2Cl_2 solution, which gradually decreased and finally reached 3.6 μ_B at 173 K. The result clearly indicates that **1**(3,5-Cl_2Py) is in an essentially pure intermediate-spin state at 298 K and that the spin state changes from the $S = 3/2$ at 298 K to the mixed $S = 3/2$ and 1/2 at 173 K. Thus, the magnetic behaviors of **1**(4-CNPy) and **1**(3,5-Cl_2Py) resemble to those of $[Fe(OETPP)Py_2]^+$ and $[Fe(OMTPP)(4\text{-}CNPy)_2]^+$, both of which exhibit the spin transition from the $S = 3/2$ to the $S = 1/2$.[39−41] In contrast to these complexes, **1**(Py) is mainly in the $S = 1/2$, even at ambient temperature since the average chemical shifts of the CH_2 signals at 298 K is 10.8 ppm, which is not much different from 6.7 ppm in low-spin **1**(DMAP) as listed in Table 1.

The Curie plots of **1**(THF) were different from those of **1**(4-CNPy) and **1**(3,5-Cl_2Py) because the extremely downfield-shifted CH_2 signals moved further downfield linearly at lower temperatures as shown in Figure 2a. Thus, **1**(THF) maintains the $S = 3/2$ throughout the temperature range examined by NMR spectroscopy.[39,41,50]

EPR Spectroscopy. The spin state of the iron(III) porphyrins at much lower temperature can be determined by EPR spectroscopy. High-spin complexes exhibit the $g_\perp$ and $g_{||}$ signals at ∼6.0 and 2.0, while the intermediate-spin complexes show them at ∼4.0 and 2.0.[2,5,51−53] In the case of low-spin complexes, there are three types of EPR spectra. Complexes that adopt the $(d_{xy})^2(d_{xz}, d_{yz})^3$ ground state exhibit either the rhombic or large g_{max}-type spectra depending on the orientation of planar axial ligands such as imidazole and pyridine: the complexes with parallel aligned axial ligands show the rhombic-type spectra, while those with perpendicularly aligned axial ligands show the large g_{max}-type spectra.[2] According to the recent work done by Walker and co-workers, the spectral type changes from the rhombic to the large g_{max}-type if dihedral angle between axial ligand planes exceed ∼57°.[54] In contrast, the complexes that adopt the $(d_{xz}, d_{yz})^4(d_{xy})^1$ ground state always exhibit the axial-type spectra, where $g_\perp$ values are smaller than 2.6.[2,55] The g values are good measure to determine the energy gap between the d_{xy} and d_π orbitals.[51−53] Thus, the complexes with a quite pure $(d_{xz}, d_{yz})^4(d_{xy})^1$ ground state, where the d_{xy} orbital is located far above the d_π orbitals, exhibit both $g_\perp$ and $g_{||}$ signals quite close to 2.0.[45,56]

The EPR spectra shown in Figure 6 and the g values listed in Table 2 indicate that all the complexes except **1**(THF) adopt the low-spin state with the $(d_{xy})^2(d_{xz}, d_{yz})^3$ ground state though the spectral types are different depending on the axial ligands. The complexes carrying pyridine derivatives such as **1**(DMAP), **1**(Py), **1**(4-CNPy), and **1**(3,5-Cl_2Py) exhibit the large g_{max}-type spectra. The results should be the indication that the axial ligands are taking perpendicular orientation. We originally expected that all the low-spin **1** with the $(d_{xy})^2(d_{xz}, d_{yz})^3$ ground state should give rhombic type spectra because the energy level of the d_{xz} orbital is intrinsically different from that of the d_{yz} orbital because of the presence of a nitrogen atom at one of the meso positions. Thus, the observation of the large g_{max}-type spectra suggests that the presence of a nitrogen atom does not seriously influence the spectral type of the low-spin complexes. The fact that the CN^- complex also showed the large g_{max}-type spectrum as in the case of symmetric porphyrin complexes also supports negligibly small influence of the *meso*-nitrogen atom on the EPR spectral type.[57] It should be noted, however, that both **1**(DMAP) and **1**(Py) exhibit the rhombic type spectra as well. The result can be explained in terms of the presence of two isomers where two axial ligands take parallel and perpendicular orientation at 4.2 K.[48] Consistent with the NMR results, **1**(^{t}BuNC) showed the rhombic type spectrum. This is the third example of the bis(^{t}BuNC) complex that does not exhibit the axial type spectrum in spite of the coordination of ^{t}BuNC ligand.[8,10]

1(THF) is the only example in a series of $[Fe(MAzP)L_2]^\pm$ (**1**) examined in this study that shows the intermediate-spin state even at 4 K. The $g_\perp$ signal at 4.26 suggests that the major component of this complex exists as the intermediate-spin state with ∼13% contamination of the high-spin species.[5,51]

Comparison of the Spin States of 1 with Those of 2. Figures 2 and 3 suggest that the electronic structure of **1** is surprisingly similar to that of **2** if the axial ligands are the same. Close inspection of the data in Table 1 has revealed, however, that the chemical shifts and the temperature dependence of the CH_3 signals are different between **1**(3,5-Cl_2Py) and**2**(3,5-Cl_2Py). While the CH_3 signals in **1**(3,5-Cl_2Py) appeared at 4.3 (298 K) and 4.2 ppm (223 K) in average, the corresponding signals in **2**(3,5-Cl_2Py) appeared at much more downfield positions, 6.3 (298 K) and 7.7 ppm (223 K). The results indicate that the spin population in the $d_{x^2-y^2}$ orbital in **2**(3,5-Cl_2Py) is much larger than that in **1**(3,5-Cl_2Py). In other words, the population of the $S = 5/2$ increases on going from **1**(3,5-Cl_2Py) to **2**(3,5-Cl_2Py). The Curie plots of the CH_3 signals shown in Figure 4 indicate that, while the average CH_3 signal in **1**(3,5-Cl_2Py) showed a small negative slope, that of **2**(3,5-Cl_2Py) exhibited a positive slope. The negative slope of the CH_3 signal in **1**(3,5-Cl_2Py) could be explained in terms of the spin transition from the mainly $S = 3/2$ at 298 K to the mixed $S = 3/2$ and 1/2 at 173 K as mentioned in the previous section. In contrast, the positive slope in **2**(3,5-Cl_2Py) suggests that the mixed S

(50) Sakai, T.; Ohgo, Y.; Ikeue, T.; Takahashi, M.; Takeda, M.; Nakamura, M. *J. Am. Chem. Soc.* **2003**, *125*, 13028–13029.
(51) Palmer, G. *Electron Paramagnetic Resonance of Hemoproteins. In Iron Porphyrins, Part II*; Lever, A. B. P., Gray, H. B., Eds.; Physical Bioinorganic Chemistry Series 2; Addison-Wesley: Reading, MA, 1983; pp 43−88.
(52) Bohan, T. L. *J. Magn. Reson.* **1977**, *26*, 109–118.
(53) Taylor, C. P. S. *Biochim. Biophys. Acta* **1977**, *491*, 137–148.
(54) Yatsunyk, L. A.; Dawson, A.; Carducci, M. D.; Nichol, G. S.; Walker, F. A. *Inorg. Chem.* **2006**, *45*, 5417–5428.
(55) Simonneaux, G.; Schünemann, V.; Morice, C.; Carel, L.; Toupet, L.; Winkler, H.; Trautwein, A. X.; Walker, F. A. *J. Am. Chem. Soc.* **2000**, *122*, 4366–4377.
(56) Moore, K. T.; Fletcher, J. T.; Therien, M. J. *J. Am. Chem. Soc.* **1999**, *121*, 5196–5209.
(57) Inniss, D.; Soltis, S. M.; Strouse, C. E. *J. Am. Chem. Soc.* **1988**, *110*, 5644–5650.

Table 3. ^{1}H NMR Chemical Shift of [Fe(Por)(^{t}BuNC)$_2$]$^+$ Taken in CD_2Cl_2 at 298 K

Por[a]	electronic ground state	α-CH_2	α-CH_3	*meso*-H	^{t}BuNC
OEP[b]	$(d_{xz}, d_{yz})^4(d_{xy})^1$	7.6		−37.7	−0.8
MAzP	$(d_{xy})^2(d_{xz}, d_{yz})^3$	14.2, 14.4 14.6, 15.3		9.8, 11.5	2.5[c]
DAzP[b]	$(d_{xy})^2(d_{xz}, d_{yz})^3$	17.9	35.3	19.2	3.5[c]

[a] Structural formulas are given in Scheme 1. [b] As reported, the chemical shifts of the α-CH_2 and α-CH_3 signals listed in the original manuscript are mistyped.[8] [c] Extraporated value.

= 3/2 and 5/2 spin state is maintained even at 173 K.[58,59] The EPR spectra support the conclusion because **1**(3,5-Cl_2Py) showed the $S = 1/2$, while **2**(3,5-Cl_2Py) exhibited the mixed $S = 3/2$ (major) and 5/2 (minor) at 4 K; the $g_\perp$ values were 3.46 and 4.23, respectively, in frozen CH_2Cl_2 solution.[58] The low-spin state in **1**(3,5-Cl_2Py) at 4 K can be explained in terms of the destabilization of the $d_{x^2-y^2}$ orbital caused by the smaller N4 cavity of the MAzP core as compared with the OEP core. In fact, the X-ray crystallographic analysis reported by Balch and co-workers has revealed that the average Fe−N_p bond in Fe(MAzP)Cl is 2.044 Å,[16] which is ∼0.02 Å shorter than that in Fe(OEP)Cl.[60]

Comparison of the Electronic Ground State of 1(^{t}BuNC) with That of Other Bis(^{t}BuNC) Complexes. Another notable difference has been observed in the ^{t}BuNC complexes. While **1**(^{t}BuNC) exhibits the $(d_{xy})^2(d_{xz}, d_{yz})^3$ ground state, most of the other bis(^{t}BuNC) complexes, including **2**(^{t}BuNC) adopt the $(d_{xz}, d_{yz})^4(d_{xy})^1$ ground state. Thus, the introduction of a nitrogen atom at the meso position stabilizes the $(d_{xy})^2(d_{xz}, d_{yz})^3$ ground state. As mentioned, we have already reported that the diazaporphyrin complex, [Fe(DAzP)(^{t}BuNC)$_2$]$^+$(see Scheme 1), is the first example showing the $(d_{xy})^2(d_{xz}, d_{yz})^3$ ground state in spite of the coordination of ^{t}BuNC.[8] These results suggest that the introduction of only one nitrogen atom in place of a *meso*-carbon atom is sufficient enough to convert the electronic ground state from $(d_{xz}, d_{yz})^4(d_{xy})^1$ to $(d_{xy})^2(d_{xz}, d_{yz})^3$. The stabilization of the $(d_{xy})^2(d_{xz}, d_{yz})^3$ ground state should be ascribed at least partly to the smaller N4 cavities in the MAzP and DAzP cores as compared with the OEP core. Thus, the smaller N4 cavity in **1** strengthens the interactions between the d_π orbitals of iron(III) and the HOMO−3 and HOMO−4 in MAzP. These interactions should be further strengthened in **1**(^{t}BuNC) because the iron(III) ion is electron deficient as compared with that in **1**(DMAP) because of the strong π-back-donation from the iron(III) to the ^{t}BuNC ligand. Consequently, the d_π orbitals are destabilized to the positions that are located above the d_{xy} orbital even in the presence of ^{t}BuNC, leading to the formation of the $(d_{xy})^2(d_{xz}, d_{yz})^3$ ground state.

In Table 3, the chemical shifts of the bis(^{t}BuNC) complexes of OEP, MAzP, and DAzP are given. As the number of nitrogen atom increases, the *meso*-H signals have moved from −37.7 to 10.9 (av) and then to 19.2 ppm, suggesting the decrease in spin density at the *meso*-carbon atoms from a large positive value in [Fe(OEP)(^{t}BuNC)$_2$]$^+$ to a large negative value in [Fe(DAzP)(^{t}BuNC)$_2$]$^+$; the spin density at the *meso*-carbon atoms in the latter complex was determined to be −0.012 on the basis of the NMR data.[8] Similar to the *meso*-H signals, the α-CH_2 signals have also moved downfield from 7.6 to 14.6 and then to 17.9 ppm, suggesting the increase in spin density on the pyrrole β carbon atoms. Since the dipolar shifts (δ_{dip}) of the peripheral protons in low-spin $(d_{xy})^2(d_{xz}, d_{yz})^3$ complexes are negative, the contact shift(δ_{con}) of the *meso*-H and α-CH_2 signals, which reflects the spin densities on the *meso*- and pyrrole β-carbon atoms, must be much larger than the estimated isotropic shifts (δ_{iso}) as the equation given below suggests

$$\delta_{con} = \delta_{iso} - \delta_{dip} > \delta_{iso} \quad (1)$$

Then, the question arises as to why the spin density on the pyrrole β and meso positions in **1**(^{t}BuNC) are quite different from those in the other low-spin complexes such as **1**(DMAP) and **1**(CN^-), although they commonly adopt the $(d_{xy})^2(d_{xz}, d_{yz})^3$ ground state. As mentioned, the increase in positive spin on the pyrrole β carbon atoms should be ascribed to the stronger interactions between the half-filled d_π and filled HOMO−3 or HOMO−4 in [Fe(MAzP)(^{t}BuNC)$_2$]$^+$ as compared with those in [Fe(MAzP)(DMAP)$_2$]$^+$. As the DFT calculation suggests, the molecular orbitals of zinc(porphin) are stabilized by the replacement of an electronegative nitrogen atom in place of a carbon atom. Especially stabilized are the HOMO−1, LUMO, and LUMO+1 because these orbitals have large coefficients at the meso positions. In contrast, the HOMO−3 and HOMO−4 orbitals having zero coefficient at the meso positions are less affected by the nitrogen atom introduced to the meso position. Consequently, the interactions between the d_π and LUMO or LUMO+1 are strengthened, while those between the iron d_π and the HOMO−3 and HOMO−4 are maintained by the introduction of the nitrogen atom to the meso position. Thus, the half-filled iron d_π orbitals can interact both with the filled HOMO−3 and HOMO−4 orbitals and the empty LUMO and LUMO+1 orbitals. In this situation, if axial DMAP is replaced by ^{t}BuNC having low-lying π^* orbitals, the iron(III) ion should be electron deficient. As a result, strong electron donation should occur from the HOMO−3 or HOMO−4 to the iron d_π orbital, which results in the increase in spin density at the pyrrole β positions. The large negative spin on the *meso*-carbon atoms in **1**(^{t}BuNC) could be explained if we assume the presence of thermally accessible excited state where MAzP adopts the open shell singlet; the HOMO−3 has positive spin while the LUMO has negative spin. Obviously, both the theoretical and experimental studies are necessary to fully understand the reasons for the considerable amount of negative spin at the *meso*-carbon atoms in [Fe(MAzP)(^{t}BuNC)$_2$]$^+$ and [Fe(DAzP)(^{t}BuNC)$_2$]$^+$, which is now in progress in this laboratory.

(58) Scheidt, W. R.; Osvath, S. R.; Lee, Y. J.; Reed, C. A.; Shaevitz, B.; Gupta, G. P. *Inorg. Chem.* **1989**, *28*, 1591–1595.
(59) Kintner, E. T.; Dawson, J. H. *Inorg. Chem.* **1991**, *30*, 4892–4897.
(60) Ernst, J.; Subramanian, J.; Fuhrhop, J.-H. *Z. Naturforsch.* **1977**, *32a*, 1129–1136.
(61) Safo, M. K.; Gupta, G. P.; Walker, F. A.; Scheidt, W. R. *J. Am. Chem. Soc.* **1991**, *113*, 5497–5510.
(62) Masuda, H.; Taga, T.; Osaki, K.; Sugimoto, H.; Yoshida, Z.; Ogoshi, H. *Bull. Chem. Soc. Jpn.* **1982**, *55*, 3891–3895.

Conclusion

Electronic structures of a series of $[Fe(MAzP)L_2]^{\pm}$ (**1**) and $[Fe(OEP)L_2]^{\pm}$ (**2**) have been examined by ^1H NMR and EPR spectroscopy. For various axial ligands, the electronic structures are quite similar between **1** and **2**.

Major differences are as follows: (1) While **2**(^{t}BuNC) adopts the $(d_{xz}, d_{yz})^4(d_{xy})^1$ ground state as in the case of most of the bis(^{t}BuNC) complexes reported previously, **1**(^{t}BuNC) exhibits the $(d_{xy})^2(d_{xz}, d_{yz})^3$ ground state. (2) While **2**(3,5-Cl_2Py) maintains the $S = 3/2$ with minor contribution of the $S = 5/2$ in a wide range of temperature, **1**(3,5-Cl_2Py) shows the spin transition from the mainly $S = 3/2$ at 298 K to the pure $S = 1/2$ at 4 K. These differences have been ascribed to the narrow N4 cavity, and the stabilization of the LUMO in the MAzP core as compared with the OEP core, both of which are caused by the replacement of a *meso*-carbon by the nitrogen atom.

Acknowledgment. Thanks are due to the Research Center for Molecular-Scale Nanoscience, the Institute for Molecular Science (IMS). This work was supported by Research Center for Materials with Integrated Properties, Toho University, Funabashi, 274-8510, Japan.

Supporting Information Available: ^1H NMR spectra and Curie plots of the CH_2 signals of **1**(1-MeIm), **1**(CN^-), and **1**(Py). This material is available free of charge via the Internet at http://pubs.acs.org.

IC800674D